

# Retrieval of Aerosol Optical Depth (AOD) using NOAA AVHRR data in an Alpine Environment

Adrian Hauser, David Oesch, Stefan Wunderle

Remote Sensing Research Group, Departement of Geography, University of Bern,  
Hallerstrasse 12, 3012 Bern, Switzerland

## ABSTRACT

The aim of this study is the retrieval of aerosol optical depth from the National Oceanic and Atmospheric Administration (NOAA) Advanced Very High Resolution Radiometer (AVHRR) sensor over land. The region of interest covers central Europe ranging from 50°N to 40.5°N and from 0°E to 17°E including the European Alps. On the temporal scale, we limit the data set to afternoon NOAA-16 passes of the entire year 2002. In this region, there are sixteen stations from the Aerosol Robotic Network (AERONET) at which we can compare the ground based versus the space borne measurements. The most crucial parameter in the retrieval procedure is the estimate of a correct surface reflectance since inaccuracies of 0.01 can result in AOD variations of  $\pm 0.1$ . Surface reflectance has been estimated by extracting the minimum reflectance within 10° intervals of the satellite zenith angle within two-month intervals. This method eliminates the varying reflectance with varying satellite zenith angle but the extracted surface reflectance still contains an aerosol signal. Most stations show a clear relationship between the AVHRR and the AERONET data. In case of a weak or non-existing relationship, we were able to identify reasons for this behavior. The standard error of estimate is about 0.18. The largest potential to increase the accuracy of this product comes from an improvement of the cloud mask. We can conclude that aerosol retrieval over land using AVHRR is a challenging task but it is possible to extract some valuable results.

**Keywords:** Aerosol, AERONET, AVHRR, AOD

## 1. INTRODUCTION

Satellite remote sensing is for many earth observation tasks the most appropriate tool. Depending on the specific demands it offers a high spatial and/or temporal resolution. However, the intermediate atmosphere blurs the enthusiasm for many applications since it can modify a signal containing surface properties substantially. Besides the absorption and scattering caused by the different air components, aerosols play a major role in the shortwave radiation transfer in the atmosphere.

Current state of the art space borne imaging radiometers like the Moderate Resolution Imaging Spectroradiometer (MODIS) or the Multi-angle Imaging SpectroRadiometer (MISR) offer great possibilities for aerosol remote sensing. On the contrary, AVHRR offers a unique temporal coverage of over twenty years. The National Oceanic and Atmospheric Administration (NOAA) generates operational maps of the aerosol optical depth (AOD) over oceans.<sup>1</sup> Many remote sensing applications over land require AOD data, e.g. for atmospheric correction. The retrieval of AOD over land is more demanding because the surface reflectance is generally not only higher, so it provides less sensitivity to changes in aerosols, but varies spatially and temporally. Additionally, knowledge of the Bidirectional Reflectance Distribution Function (BRDF), which describes the angular reflectance properties, is required. Inaccuracies of 0.01 of the surface reflectance can result in AOD variations of  $\pm 0.1$ .<sup>2</sup>

The long term goal is to develop a procedure to estimate AOD from AVHRR suitable for real-time processing as well as for analyzing historic data. In this study we compare AOD data from AVHRR with ground based measurements from AERONET.

---

Send correspondence to Adrian Hauser

e-mail: [adrian@giub.unibe.ch](mailto:adrian@giub.unibe.ch), phone: +41 (0)31 631 8552, <http://saturn.unibe.ch/rsbern/>

Copyright 2003 Society of Photo-Optical Instrumentation Engineers. This paper will be published in SPIE International Symposium Remote Sensing 2003, Barcelona, Spain, and is made available as an electronic preprint with permission of SPIE. One print or electronic copy may be made for personal use only. Systematic or multiple reproduction, distribution to multiple locations via electronic or other means, duplication of any material in this paper for a fee or for commercial purposes, or modification of the content of the paper are prohibited.

## 2. DATA

The two data sources in this study are the NOAA AVHRR level1b data set, which has been pre-processed to provide cloud-free top of atmosphere (TOA) reflectance and aerosol optical depths from AERONET. Additionally, meteorological data (vertically integrated water vapor and sea level pressure at 12:00 UTC) from the Alpine Model (aLMo) produced by MeteoSwiss and total column ozone data (12:00 UTC) from the National Center for Environmental Prediction (NCEP) are used. In this study, we limit our data set to NOAA-16 afternoon passes of the entire year 2002.

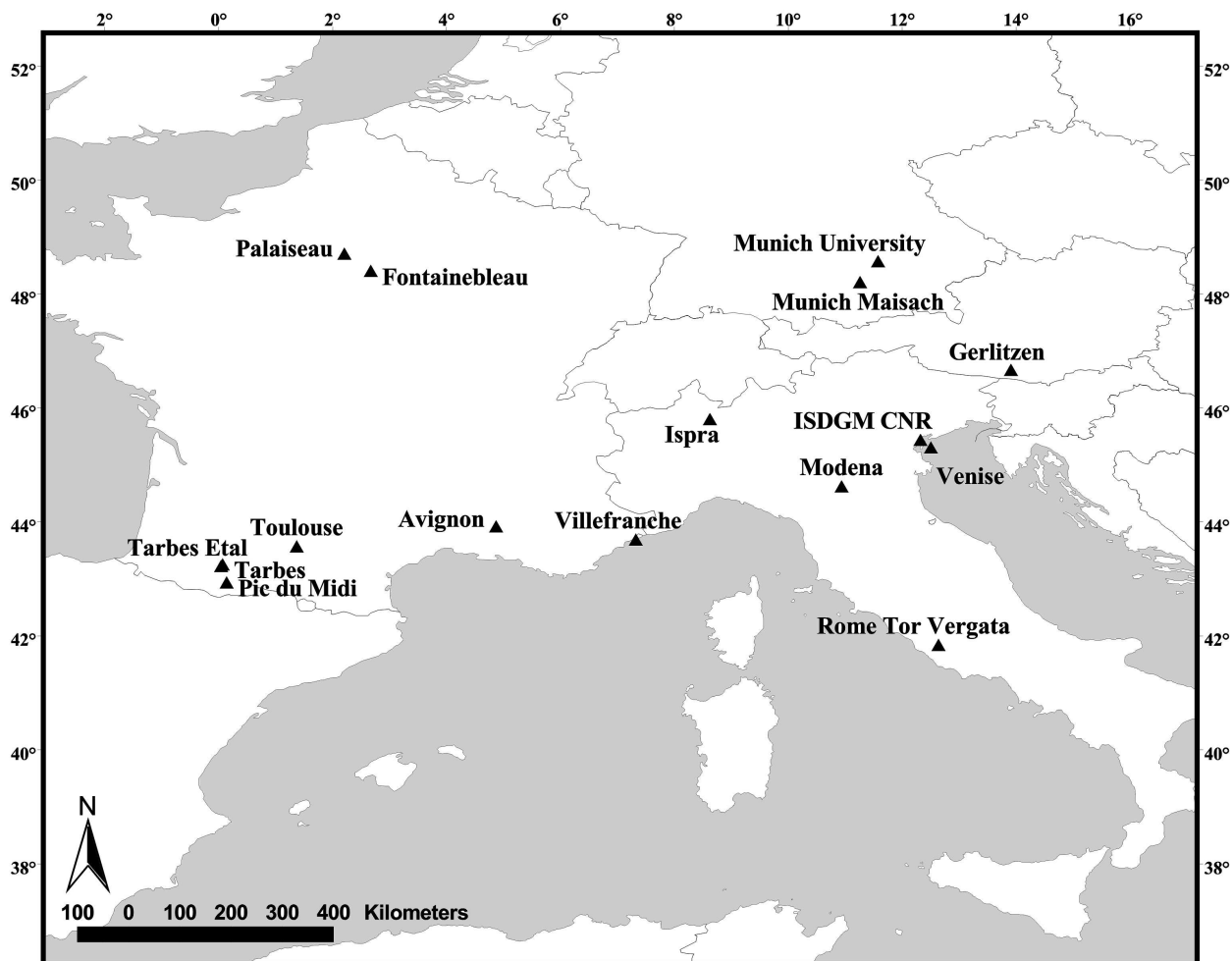


**Figure 1.** Map of central Europe showing the AERONET stations used in this study. The area of the AVHRR coverage ranges from 50°N to 40.5°N and from 0°E to 17°E.

### 2.1. AVHRR Data Set

The data presented in this paper uses observations from the 5-channel AVHRR on board the operational polar NOAA satellites. The instrument measures emitted and reflected radiance in the following bands: 0.58-0.68 (channel 1), 0.725-1.10 (channel 2), 3.55-3.93 (channel 3), 10.3-11.3 (channel 4) and 11.5-12.5 (channel 5) micrometers. The nominal instrument spatial resolution is approximately 1.1km. The NOAA AVHRR data are ingested by a receiving station located in Bern, Switzerland (46.917°N / 7.467°E). Since August 2001, we are in an operational status to receive and process all data covering the European Alps in near real-time. The dataset

in this paper consists of all NOAA-16 afternoon passes for the year 2002 and is mapped to a latitude-longitude grid, covering central Europe and the alpine region from 40.5°N to 50°N and 0°E to 17°E.

Pre-processing of NOAA-AVHRR level1b imagery for the retrieval of aerosol optical depth incorporates calibration of the visible channels 1 and 2 according to the NOAA KLM users guide.<sup>3</sup> For improving the georeferencing, a feature matching algorithm is used to geocode the satellite imagery with sub-pixel accuracy. An orthorectification of the imagery is essential in an alpine region to overcome the displacement errors introduced by the topography. An automated procedure which uses a terrain model based on the GTOPO30 was developed and implemented.

## 2.2. AERONET Data Set

The Aerosol Robotic Network (AERONET) is a world-wide federation of ground based sun-sky radiometers. The network imposes standardization of instruments, calibration and processing. The data is centrally archived and available in three processing levels (unscreened (L1.0), cloud-screened (L1.5) and cloud-screened and quality-assured (L2.0)). According to Holben,<sup>4</sup> the accuracy is about  $\pm 0.02$ . Fig. 1 shows all AERONET stations used in this study. To get a larger and consistent data set, only L1.5 data has been used because L2.0 data were only available for seven stations. The wavelengths observed by AERONET instruments include: (0.34), (0.38), 0.44, (0.50), 0.67, 0.87 and 1.02 micrometer. The wavelengths in parentheses are additional channels which are not provided by all stations. To be able to compare the AERONET data with the AVHRR AOD retrievals, the AERONET data from different wavelengths are interpolated to 0.55 micrometers using a 2<sup>nd</sup>-order polynomial fit of the logarithmic wavelengths.

## 3. AEROSOL RETRIEVAL FROM NOAA-16 AVHRR

Classical approaches to retrieve aerosol optical depth (AOD) from NOAA AVHRR use surface targets with known reflectance characteristics. These targets consist mainly of water bodies and dark dense vegetation (DDV).<sup>2,5</sup> Our region of interest is located in the middle of Europe and densely populated, dark dense vegetation targets are sparse and not uniformly distributed. Lakes with a sufficient size are also few in numbers.

In general, surface reflectance over land in channel 1 is rather low and show a significant deviation from ideal lambertian surfaces. While for a lambertian surface the surface reflectance is independent from the satellite zenith angle and from forward or backward scattering, most natural surfaces have a more complex behavior which is expressed by the Bidirectional Reflectance Distribution Function (BRDF). There are many studies and models dealing with this problem, however, the application of a BRDF model requires accurate information about the surface type which is often not available or outdated.

To omit errors introduced by an inaccurate BRDF model we try to determine the BRDF from the data itself and follow partly the ideas of Knapp and Stowe.<sup>6</sup> For each cloud-free pixel a function of the top of atmosphere reflectance versus the satellite zenith angle can be plotted. We assume that the lowest reflectance values within a certain satellite zenith angle interval represents a nearly aerosol-free observation. In this sense, the lowest reflectance values describe the reflectance deviations due to variations of the satellite zenith angle. An example for the station of Avignon, France (43.92°N / 4.87°E) is shown in Fig. 2. To account for variations of the surface reflectance we split the dataset into six two-month periods, this should at least minimize some seasonal variations of the surface reflectance. Obviously, it is not realistic to assume that over a two month period and with varying satellite zenith angles we can fulfill for all satellite zenith angles the assumption to get cloud- and aerosol-free observations. A simple calculation supports this: Over a two month period (60 images) we expect a mean cloud cover of 50%. Assuming a uniform distribution of satellite zenith angles (-70° to +70°) and intervals of 10° we can expect about 2 data points in each 10° interval. That the minimum value can be considered as aerosol-free is apparently not in all cases realistic. In wintertime, we expect more cloud cover but also less aerosols<sup>7</sup> than in summertime.

The major advantage of this method is that it allows to get an estimate of the channel 1 reflectance for all surfaces independent of their land cover type. The cloud- and aerosol-free reflectance data is then atmospherically corrected and can be called cloud- and aerosol-free surface reflectance. The radiative transfer code used for the atmospheric correction of the top of atmosphere reflectance and for the retrieval of the aerosol optical depth

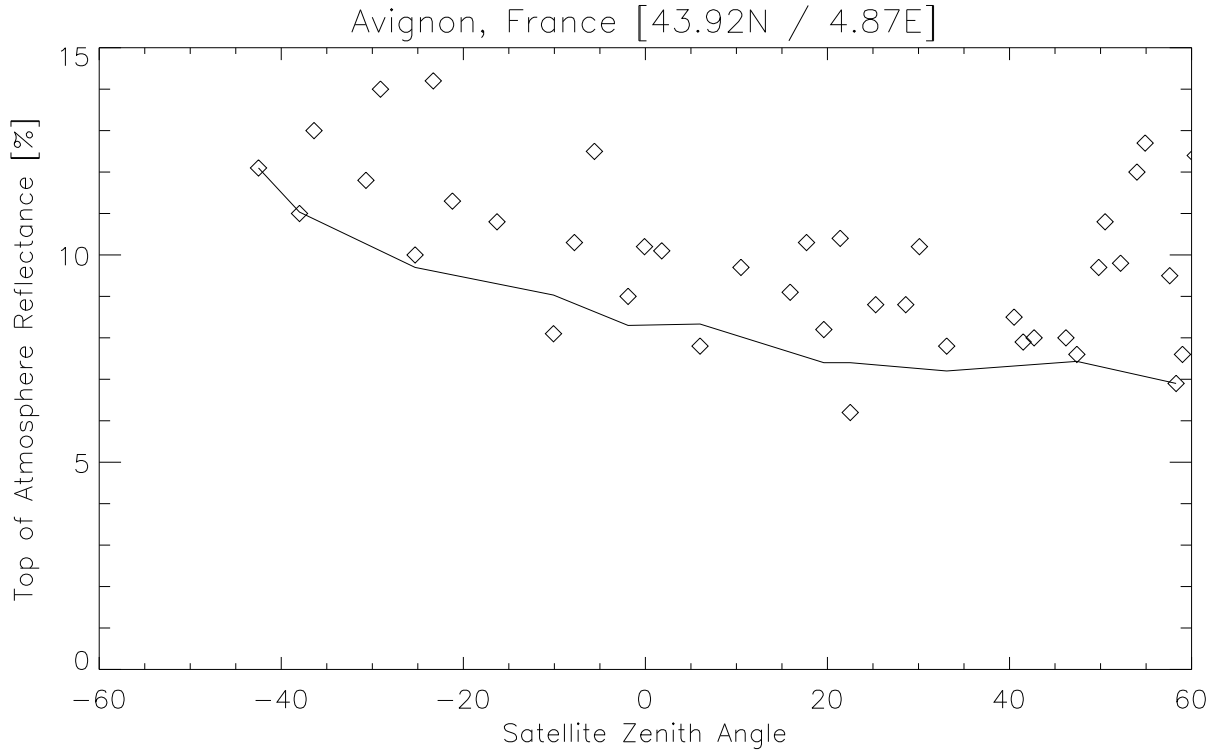


**Figure 2.** Uncorrected top of atmosphere reflectance from NOAA-16 AVHRR. Only data from July/August 2002 are shown (diamonds). The line represents the top of atmosphere reflectance for cloud-free conditions, after correcting the atmospheric interference it can be called surface reflectance. It is the result from selecting the minimum reflectance within 10 degree intervals of the satellite zenith angle and smoothing(boxcar average, width of 3). The AERONET site of Avignon is located in an agricultural region 10km east of the city of Avignon.

is the updated SMAC<sup>8</sup> algorithm. Updated means that it is no longer based on the 5S<sup>9</sup> code but on the newer version 6S.<sup>10</sup> Using SMAC, we can retrieve the aerosol optical depth using high resolution (7km × 7km) vertically integrated water vapor and surface pressure information as well as 1° × 1° ozone data for each pixel. A continental aerosol model<sup>11</sup> is expected to be most appropriate for this region.

Obviously, we expect the retrieved aerosol optical depth from AVHRR to be within a certain region spatially more or less homogeneous. Pixels are labeled as invalid data if the standard deviation of the surface reflectance within a 3 × 3 window is larger than the mean of the standard deviation of the surface reflectance of the whole image. The rationale for this pre-selection is that otherwise minor inaccuracies of the geocoding could result in a larger deviation of the surface reflectance and be misinterpreted as an aerosol signal. This procedure has been repeated in an analogous way for the aerosol optical depth to eliminate local noise. This data filtering reduces the amount of available AVHRR pixels. To fill these data gaps, the dataset has been smoothed using a 25km × 25km window.

**Table 1.** Statistical parameters of AOD retrievals from AVHRR compared to AERONET data. Columns indicate the max. time difference between the two measurements. ‘reg.’ represents an average over a 25km × 25km region while ‘pnt.’ represents only the pixel at the exact AERONET location. ‘ $r^2$ ’ is the correlation coefficient between AVHRR and AERONET data, ‘n’ is the number of cloud-free data points and ‘ $\sigma$ ’ the standard deviation of the retrieval error.

| Station           |          | 10min |      | 15min |      | 20min |      | 30min |      | 45min |      | 60min |      |
|-------------------|----------|-------|------|-------|------|-------|------|-------|------|-------|------|-------|------|
|                   |          | reg.  | pnt. | reg.  | pnt. | reg.  | pnt. | reg.  | pnt. | reg.  | pnt. | reg.  | pnt. |
| Avignon           | $r^2$    | 0.07  | 0.41 | 0.09  | 0.45 | 0.13  | 0.19 | 0.12  | 0.24 | 0.13  | 0.46 | 0.14  | 0.46 |
|                   | n        | 97    | 8    | 112   | 10   | 122   | 13   | 130   | 14   | 139   | 16   | 151   | 16   |
|                   | $\sigma$ | 0.18  | 0.07 | 0.18  | 0.07 | 0.19  | 0.11 | 0.18  | 0.12 | 0.18  | 0.11 | 0.20  | 0.11 |
| Fontainebleau     | $r^2$    | 0.36  | 0.82 | 0.17  | 0.46 | 0.21  | 0.43 | 0.21  | 0.21 | 0.27  | 0.29 | 0.23  | 0.26 |
|                   | n        | 20    | 8    | 32    | 14   | 37    | 16   | 48    | 24   | 53    | 27   | 59    | 29   |
|                   | $\sigma$ | 0.15  | 0.08 | 0.20  | 0.14 | 0.20  | 0.14 | 0.21  | 0.19 | 0.22  | 0.21 | 0.22  | 0.21 |
| Gerlitzzen        | $r^2$    | 0.96  | 1.00 | 0.96  | 1.00 | 0.11  | 1.00 | 0.81  | 1.00 | 0.77  | 1.00 | 0.77  | 1.00 |
|                   | n        | 3     | 2    | 3     | 2    | 4     | 2    | 7     | 2    | 8     | 2    | 8     | 2    |
|                   | $\sigma$ | 0.00  | 0.00 | 0.00  | 0.00 | 0.04  | 0.00 | 0.07  | 0.00 | 0.09  | 0.00 | 0.09  | 0.00 |
| ISDGM CNR         | $r^2$    | 0.46  | 0.02 | 0.40  | 0.02 | 0.35  | 0.02 | 0.35  | 0.02 | 0.33  | 0.02 | 0.28  | 0.02 |
|                   | n        | 31    | 3    | 43    | 3    | 46    | 3    | 57    | 3    | 62    | 3    | 70    | 3    |
|                   | $\sigma$ | 0.18  | 0.24 | 0.18  | 0.24 | 0.20  | 0.24 | 0.20  | 0.24 | 0.20  | 0.24 | 0.21  | 0.24 |
| Ispra             | $r^2$    | 0.58  | 0.48 | 0.64  | 0.47 | 0.61  | 0.48 | 0.60  | 0.49 | 0.51  | 0.49 | 0.50  | 0.49 |
|                   | n        | 83    | 26   | 94    | 30   | 103   | 31   | 117   | 32   | 125   | 32   | 130   | 32   |
|                   | $\sigma$ | 0.13  | 0.13 | 0.12  | 0.12 | 0.13  | 0.12 | 0.13  | 0.12 | 0.15  | 0.12 | 0.16  | 0.12 |
| Modena            | $r^2$    | 0.00  | 1.00 | 0.09  | 0.03 | 0.06  | 0.02 | 0.08  | 0.02 | 0.19  | 0.04 | 0.16  | 0.04 |
|                   | n        | 33    | 3    | 46    | 5    | 55    | 6    | 61    | 6    | 67    | 7    | 70    | 7    |
|                   | $\sigma$ | 0.18  | 0.00 | 0.19  | 0.20 | 0.19  | 0.20 | 0.20  | 0.20 | 0.21  | 0.20 | 0.21  | 0.20 |
| Munich Maisach    | $r^2$    | 0.01  | 0.16 | 0.01  | 0.16 | 0.02  | 0.16 | 0.08  | 0.16 | 0.10  | 0.16 | 0.09  | 0.16 |
|                   | n        | 24    | 3    | 30    | 3    | 33    | 3    | 40    | 3    | 50    | 3    | 53    | 3    |
|                   | $\sigma$ | 0.18  | 0.13 | 0.17  | 0.13 | 0.17  | 0.13 | 0.18  | 0.13 | 0.20  | 0.13 | 0.21  | 0.13 |
| Munich University | $r^2$    | –     | –    | 0.02  | –    | 0.06  | –    | 0.06  | –    | 0.09  | 1.00 | 0.09  | 1.00 |
|                   | n        | –     | –    | 9     | 1    | 10    | 1    | 10    | 1    | 12    | 2    | 12    | 2    |
|                   | $\sigma$ | –     | –    | 0.11  | –    | 0.10  | –    | 0.10  | –    | 0.09  | 0.00 | 0.09  | 0.00 |
| Palaiseau         | $r^2$    | 0.22  | 1.00 | 0.31  | 0.99 | 0.50  | 0.99 | 0.50  | 0.99 | 0.52  | 0.99 | 0.40  | 0.49 |
|                   | n        | 12    | 2    | 14    | 3    | 16    | 4    | 18    | 4    | 19    | 4    | 24    | 7    |
|                   | $\sigma$ | 0.16  | 0.00 | 0.16  | 0.02 | 0.15  | 0.02 | 0.15  | 0.02 | 0.15  | 0.02 | 0.22  | 0.16 |
| Pic du Midi       | $r^2$    | 0.11  | 1.00 | 0.11  | 1.00 | 0.11  | 1.00 | 0.14  | 1.00 | 0.08  | 1.00 | 0.08  | 1.00 |
|                   | n        | 10    | 2    | 10    | 2    | 10    | 2    | 11    | 2    | 12    | 2    | 13    | 2    |
|                   | $\sigma$ | 0.31  | 0.00 | 0.31  | 0.00 | 0.31  | 0.00 | 0.30  | 0.00 | 0.31  | 0.00 | 0.30  | 0.00 |
| Rome Ter Vergata  | $r^2$    | 0.17  | 0.04 | 0.17  | 0.04 | 0.20  | 0.13 | 0.41  | 0.34 | 0.44  | 0.54 | 0.42  | 0.54 |
|                   | n        | 34    | 7    | 42    | 7    | 49    | 8    | 54    | 9    | 59    | 10   | 62    | 10   |
|                   | $\sigma$ | 0.17  | 0.12 | 0.16  | 0.12 | 0.15  | 0.15 | 0.15  | 0.14 | 0.15  | 0.14 | 0.15  | 0.14 |
| Tarbes            | $r^2$    | 0.32  | –    | 0.29  | 0.44 | 0.22  | 0.23 | 0.22  | 0.23 | 0.22  | 0.23 | 0.22  | 0.23 |
|                   | n        | 8     | 1    | 10    | 3    | 11    | 4    | 11    | 4    | 11    | 4    | 11    | 4    |
|                   | $\sigma$ | 0.17  | –    | 0.16  | 0.11 | 0.16  | 0.11 | 0.16  | 0.11 | 0.16  | 0.11 | 0.16  | 0.11 |
| Tarbes Etal       | $r^2$    | 0.15  | 0.53 | 0.23  | 0.80 | 0.21  | 0.54 | 0.13  | 0.56 | 0.08  | 0.53 | 0.10  | 0.49 |
|                   | n        | 43    | 10   | 48    | 12   | 57    | 14   | 64    | 17   | 73    | 18   | 77    | 19   |
|                   | $\sigma$ | 0.24  | 0.08 | 0.24  | 0.07 | 0.16  | 0.11 | 0.25  | 0.11 | 0.27  | 0.12 | 0.27  | 0.12 |
| Toulouse          | $r^2$    | 0.00  | 0.01 | 0.00  | 0.00 | 0.00  | 0.00 | 0.00  | 0.00 | 0.00  | 0.00 | 0.00  | 0.00 |
|                   | n        | 38    | 9    | 44    | 12   | 47    | 13   | 52    | 13   | 55    | 13   | 56    | 14   |
|                   | $\sigma$ | 0.24  | 0.26 | 0.23  | 0.23 | 0.25  | 0.25 | 0.24  | 0.25 | 0.25  | 0.25 | 0.25  | 0.24 |
| Venice            | $r^2$    | 0.38  | 0.39 | 0.36  | 0.42 | 0.34  | 0.35 | 0.24  | 0.33 | 0.14  | 0.33 | 0.09  | 0.33 |
|                   | n        | 48    | 22   | 58    | 28   | 64    | 31   | 68    | 32   | 75    | 33   | 81    | 33   |
|                   | $\sigma$ | 0.17  | 0.11 | 0.16  | 0.10 | 0.16  | 0.11 | 0.18  | 0.11 | 0.19  | 0.11 | 0.20  | 0.11 |
| Villefranche      | $r^2$    | 0.23  | 0.78 | 0.26  | 0.70 | 0.25  | 0.52 | 0.23  | 0.40 | 0.25  | 0.39 | 0.25  | 0.42 |
|                   | n        | 26    | 12   | 31    | 14   | 37    | 16   | 39    | 17   | 42    | 18   | 43    | 19   |
|                   | $\sigma$ | 0.12  | 0.08 | 0.12  | 0.10 | 0.12  | 0.14 | 0.12  | 0.15 | 0.12  | 0.15 | 0.12  | 0.15 |

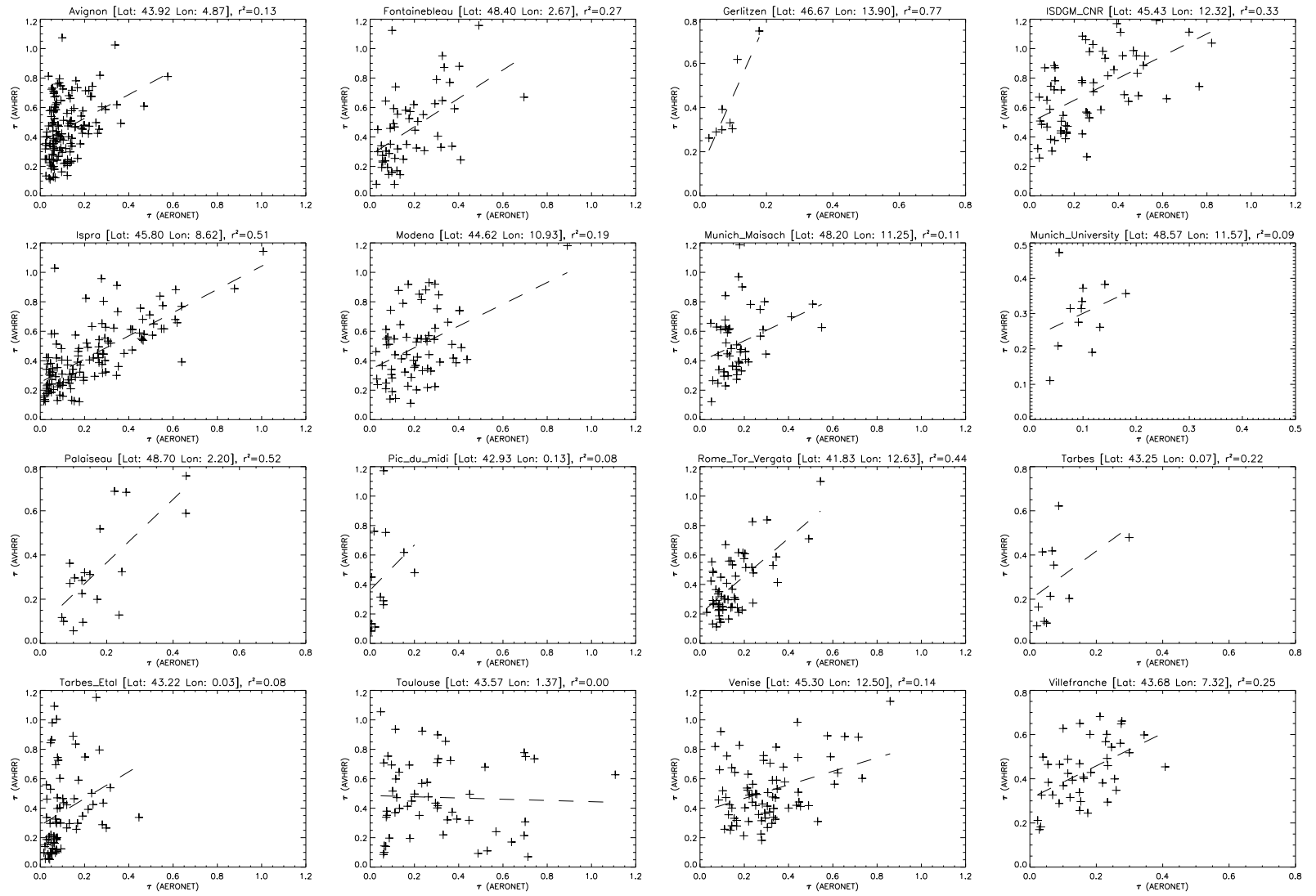


**Figure 3.** Aerosol optical depth retrieved from NOAA-16 AVHRR versus AERONET measurements for the year 2002. The maximum time difference between the two measurements is 45 minutes.

## 4. RESULTS

A comparison of ground based AERONET measurements with AVHRR retrievals includes a potential source of uncertainty due to different spatial and temporal scales.<sup>12</sup> One would expect that the spatial scale should be minor since full resolution AVHRR is used. This is not the case when comparing the smoothed dataset to AERONET measurements. Choosing the most appropriate maximum time delay between two measurements is difficult. Table 1 lists the correlation coefficients, number of observations and standard deviations of the error for different maximum time slots. In general, the number of observations decreases with decreasing time slots but the correlation coefficient and the standard deviation of the error in Table 1 do not necessarily improve. Narrow time slots reduce the risk to include cloud contaminated data since the cloud masking from AVHRR is much more difficult and inaccurate than cloud masking from AERONET but outlying data points can not be avoided in total (Fig. 3).

We conclude from Table 1 that the maximum time difference between the AVHRR and AERONET retrievals should not exceed 45 minutes. A maximum time difference of 10 or 15 minutes reduces the number of measurements to a too large extent. At 45 minute measure interval, five out of sixteen stations reach the maximum correlation coefficient for the interpolated data.

The scatter plots of the AVHRR versus the AERONET measurements are shown in Fig. 3. This figure includes all cloud-free data points averaged over an area of  $25\text{km} \times 25\text{km}$ . The number of data points plotted in each chart varies substantially from station to station. The most obvious feature of Fig. 3 is the large amount of scatter. The data is mainly distributed above the bisecting line and even shows at some stations a clear lower limit (e.g. Avignon, ISDGM CNR, Ispra, Munich Maisach, Rome Tor Vergata). The average intercept of the linear fit is about 0.30 while the standard deviation of the error for all AVHRR-AERONET data pairs is about 0.18. The pixel-wise BRDF corrected surface reflectance includes not only dark pixels like the dark dense vegetation method but instead the surface reflectance can exceed values of 10%. This affects the sensitivity to changes in aerosol adversely. The lack of a distinct upper limit of AVHRR retrieved AOD values leads to the conclusion that the cloud masking was not always successful.

Nevertheless, most stations show a clear trend even when the correlation coefficient remains rather low. This is also partly caused by the fact that the AOD measured at the AERONET stations exhibit only little variability (e.g. Gerlitzén, Munich University, Pic du Midi, Tarbes). Toulouse is the only station which shows no trend at all. A closer investigation of the AERONET data reveals that the pixels which lie well below the bisecting line also exhibit a very distinct Angstrom coefficient compared to the rest of the Toulouse data set.

## 5. DISCUSSION AND CONCLUSION

Fig. 2, Fig. 3 and Table 1 revealed some problems which have varying influence on the retrieval of AOD from AVHRR over heterogeneous land surfaces:

1. Instrumental errors like sensor noise, calibration, etc.

It is well known that the signal to noise ratio of the AVHRR sensor is rather low compared to the latest space borne imaging radiometers. Also the calibration is more difficult due to a missing in-flight calibration. Ignatov and Stowe<sup>13</sup> reported a 20% decrease in aerosol optical depth over a sixteen month period over the ocean. This decrease is likely to be at least partly induced by a drift of the calibration.

2. Retrieval uncertainties

Retrieval uncertainties contain possible error sources during the retrieval. This includes inaccuracies of the water vapor, ozone and pressure data as well as the selection of an appropriate aerosol model. The example of Toulouse in Fig. 3 illustrates the consequences of such an application.

3. Cloud masking

Ignatov and Stowe<sup>13</sup> state that “With little doubt, cloud screening is of comparable (if not greater) importance for accurate remote sensing than the aerosol retrieval algorithm itself.” We can confirm this statement with our data.

#### 4. Surface reflectance

The use of a pixel-wise BRDF corrected surface reflectance seems to be a feasible way to retrieve aerosol optical depth over land. Most former studies<sup>2</sup> have been restricted to positive satellite zenith angles (forward scattering) to limit the effects of BRDF. This limitation is not necessary when using a pixel-wise BRDF corrected surface reflectance. Additionally, this method is not restricted to specific land cover types like the widely used AOD retrieval over dark dense vegetation targets. However, the procedure needs still some further adjustments. So far, the surface reflectance still contains a significant aerosol signal which should be minimized. This results in a lower AVHRR retrieved AOD compared to the AERONET measurements.

According to Holben,<sup>4</sup> the accuracy of AERONET measurements should be  $\pm 0.02$ . To compare AVHRR and AERONET results, the AERONET data has been interpolated to the same wavelength as the AOD from AVHRR. This might incorporate additional errors. Depending on the relative azimuth angle of the system sun-satellite, it is also possible that the AERONET instrument and the AVHRR are estimating the AOD from different air masses. This error is gaining importance in the backward scattering direction.

Totalling the results of this study, we can conclude that aerosol retrieval over land using AVHRR is a challenging task but it is possible to extract some valuable results. When incorporating a pixel-wise BRDF corrected surface reflectance, the covered area can be extended compared to classical approaches. Also, restricting the AVHRR data set to forward scattering look angles is obsolete. Direct comparison of AVHRR retrieved AOD versus AERONET data yields a large amount of scatter but generally a clear trend is visible. In the future, we hope to decrease scatter by refining the cloud masking scheme. This should possess the largest potential for a further improvement of the retrieval accuracy.

### ACKNOWLEDGMENTS

We would like to thank MeteoSwiss as well as the National Center for Environmental Prediction (NCEP) for supplying meteorological data. Additionally, we thank the AERONET PIs and their staff for establishing and maintaining the sites used in this study. This study has been funded by the Swiss Defense Procurement Agency.

### REFERENCES

1. L. Stowe, A. Ignatov, and R. Singh, "Second generation operational aerosol product at NOAA/NESDIS," *Journal of Geophysical Research* **102**(D14), pp. 16923–16934, 1997.
2. V. Soufflet, D. Tanre, A. Royer, and N. T. O'Neill, "Remote sensing of aerosols over boreal forest and lake water from AVHRR data," *Remote Sensing of Environment* **60**, pp. 22–34, 1997.
3. G. Goodrum, K. B. Kidwell, and W. Winston, "NOAA KLM user's guide," Technical Report, National Environmental Satellite Data and Information Services (NESDIS), NOAA, 1998.
4. B. N. Holben, T. Eck, I. Slutsker, D. Tanre, J. P. Buis, A. Setzer, E. Vermote, J. A. Reagan, Y. J. Kaufman, T. Nakajima, F. Lavenue, I. Jankowiak, and A. Smirnov, "AERONET- a federated instrument network and data archive for aerosol characterization," *Remote Sensing of Environment* **66**, pp. 1–16, 1998.
5. Y. J. Kaufman and C. Sendra, "Algorithm for automatic atmospheric corrections to visible and near-IR satellite imagery," *International Journal of Remote Sensing* **9**(8), pp. 1357–1381, 1988.
6. K. Knapp and L. Stowe, "Deriving an aerosol optical depth climatology over land with AVHRR data," in *International Radiation Symposium*, (St. Petersburg, Russia), 2000.
7. T. Ingold, C. Mätzler, and N. Kämpfer, "Aerosol optical depth measurements by means of a sun-photometer network in Switzerland," *Journal of Geophysical Research* **106**(D21), pp. 27537–27554, 1999.
8. H. Rahman and G. Dedieu, "SMAC: A simplified method for the atmospheric correction of satellite measurements in the solar spectrum," *International Journal of Remote Sensing* **15**(1), pp. 123–143, 1994.
9. D. Tanre, C. Deroo, P. Duhaut, M. Herman, J. Morcette, J. Perbos, and P. Deschamps, "Description of a computer code to simulate the satellite signal in the solar spectrum: the 5S code.," *International Journal of Remote Sensing* **11**, pp. 659–668, 1990.

10. E. Vermote, D. Tanré, J. L. Deuze, and J. J. Morcrette, "Second simulation of satellite signal in the solar spectrum, 6S: an overview.," *IEEE Transactions on Geoscience and Remote Sensing* **35**, pp. 675–686, 1997.
11. G. D'Almeida, P. Koepke, and E. Shettle, *Atmospheric Aerosols: Global Climatology and Radiative Characteristics*, A. Deepak, Hampton, VA, USA, 561 pp, 1991.
12. K. R. Knapp and L. L. Stowe, "Evaluating the potential for retrieving aerosol optical depth over land from AVHRR Pathfinder atmosphere data.," *Journal of the Atmospheric Sciences* **59**(3), pp. 279–293, 2002.
13. A. Ignatov and L. Stowe, "Aerosol retrievals from individual AVHRR channels. Part II: Quality control, probability distribution functions, information content, and consistency checks of retrievals," *Journal of the Atmospheric Sciences* **59**(3), pp. 335–362, 2002.